Dynamical correlation functions for the one-dimensional Bose-Hubbard insulator

Kevin zu Münster and Florian Gebhard
Fachbereich Physik, Philipps Universität Marburg, D-35032 Marburg, Germany

Satoshi Ejima and Holger Fehske
Institut für Physik, Ernst-Moritz–Arndt Universität Greifswald, D-17489 Greifswald, Germany

(Received 31 March 2014; published 27 June 2014)

We calculate the dynamical current and kinetic-energy correlation functions for the first Mott lobe of the one-dimensional Bose-Hubbard model. We employ the strong-coupling expansion up to sixth order in $x = t/U$ and the dynamical density-matrix renormalization group method on rings with 64 sites. The correlation functions are finite above the single-particle gap with a square-root onset, as also found from field theory close to the Mott transition. The correlation functions display a featureless superposition of the primary and tertiary Hubbard bands. We find very good agreement between all methods in the interaction and frequency regimes where they are applicable.

DOI: 10.1103/PhysRevA.89.063623 PACS number(s): 67.85.Bc, 67.85.De, 64.70.Tg

I. INTRODUCTION

Ultracold atomic systems in which the atoms are trapped on an optical lattice offer a wide range of possibilities to prove the applicability of theoretical studies [1]. New experimental techniques such as the modulation of the amplitude and the phase of the lattice potential provide a variety of new possibilities, e.g., the modulation of the lattice potential can be used to introduce artificial gauge fields into the system [2,3]. Such a modulation derives an excitation of the system described by the kinetic and current correlation functions. Recently, the signature of a Higgs amplitude mode in the two-dimensional superfluid in the vicinity of a quantum phase transition to a Mott insulator has been predicted by field theory combined with quantum Monte Carlo simulations, showing a resonance-like feature in dynamical spectra [4]. Albeit this increasing attention, theoretical studies for these dynamical correlation functions in the bosonic systems are rare even in one dimension. Kühner *et al.* computed the optical conductivities in the one-dimensional Bose-Hubbard model by using the density-matrix renormalization group (DMRG) method [4]. The dynamical response due to the lattice modulation were also simulated by applying the time-dependent DMRG [5].

In this work we address the one-dimensional Bose-Hubbard model in the insulating phase when the number N of bosons equals the number of lattice sites L. The model describes a system of neutral spinless atoms trapped in an optical lattice with deep lattice potentials. The Bose-Hubbard Hamiltonian is defined by

$$\begin{aligned} \hat{H} &= -t\hat{T} + U\hat{D}, \\ \hat{T} &= \sum_{j=1}^{L} (\hat{b}_j^\dagger \hat{b}_{j+1} + \hat{b}_{j+1}^\dagger \hat{b}_j), \\ \hat{D} &= \frac{1}{2}\sum_{j=1}^{L} \hat{n}_j(\hat{n}_j - 1). \end{aligned} \tag{1}$$

Here, $\hat{b}_j^\dagger$, $\hat{b}_j$, and $\hat{n}_j = \hat{b}_j^\dagger \hat{b}_j$ are the boson creation, annihilation, and particle number operators on site j, respectively, and periodic boundary conditions (PBCs) apply. Throughout this work, we denote the ratio of the hopping amplitude t and the local interaction strength U by $x = t/U$.

At integer filling, $\rho = N/L = 1$, the Bose-Hubbard model describes a phase transition from the Mott insulating phase to the superfluid phase at a critical interaction ratio, $x_c \approx 0.305$ [6]. The phase transition lies in the XY universality class and is of Kosterlitz-Thouless type, which results in an exponentially small band gap near the transition. In this work we restrict ourselves to the first Mott lobe: $x < x_c$.

The response of the bosons to weak phase and amplitude modulations of the lattice potential is described by the correlation functions for the current operator and the kinetic-energy operator; for a detailed discussion of the connection between measurable quantities like the energy absorption rate and correlation functions in terms of a linear response theory, see Refs. [7–9]. We define the correlation function of an operator $\hat{A}$ as the imaginary part of the corresponding retarded Green function, which is given in frequency space by

$$\begin{aligned} \widetilde{S}_A(\omega \geqslant 0) &= -\frac{1}{\pi}\lim_{\eta\to 0^+} \mathrm{Im}\left[G_A^{\mathrm{ret}}(\omega + i\eta)\right] \\ &= \frac{1}{L}\sum_n |\langle\Psi_n|\hat{A}|\Psi_0\rangle|^2 \delta(\omega - (E_n - E_0)). \end{aligned} \tag{2}$$

Here, $|\Psi_0\rangle$ is the ground state of $\hat{H}$ with energy E_0, and $|\Psi_n\rangle$ are eigenstates of $\hat{H}$ with energy E_n. Note that the correlation functions are positive, $\widetilde{S}_A(\omega) \geqslant 0$. Moreover, the sum rule

$$\int_0^\infty d\omega \widetilde{S}_A(\omega) = \frac{1}{L}\langle\Psi_0|\hat{A}^2|\Psi_0\rangle \tag{3}$$

shows that $\widetilde{S}_A(\omega \to \infty) \to 0$.

In this work, we focus on the correlation function for the kinetic energy, $\widetilde{S}_T(\omega)$ with $\hat{T}$ from Eq. (1), and define

$$\widetilde{S}_T(\omega) = w_0^T \delta(\omega) + S_T(\omega), \tag{4}$$

where we extracted the δ peak at $\omega = 0$. Moreover, we address $S_J(\omega)$ with the current operator

$$\hat{J} = i\sum_l (b_{j+1}^\dagger b_j - b_j^\dagger b_{j+1}). \tag{5}$$

Note that S_J is related to the real part of the optical conductivity at zero momentum as [10]

$$S_J(\omega > 0) = \frac{\omega}{\pi} \mathrm{Re}[\sigma(q = 0, \omega)]. \tag{6}$$

Since we focus on the insulating phase, we know that $w_0^J = 0$ so that $\widetilde{S}_J(\omega) = S_J(\omega)$.

Our work is organized as follows: In Sec. II we briefly discuss the dynamical DMRG (DDMRG) method and the strong-coupling expansion and give the field-theory expression for the current correlation function. In Sec. III we discuss the results for the current and kinetic-energy correlation functions in the Mott phase. Conclusions and outlook, Sec. IV, close our presentation. Some technical aspects are deferred to the Appendix.

II. METHODS

We evaluate the correlation functions with the numerical DDMRG method and the analytical strong-coupling expansion (SC). We used these methods previously [11–13] for the evaluation of single-particle and two-particle response functions such as the density correlation function $S_n(k,\omega)$. In Refs. [11,13], a detailed explanation of the methods can be found. In this section, we briefly summarize the most important aspects of both methods. For comparison, we also give the field-theoretical expression for the current correlation function. For an early application of the DMRG correction vector method [14] to the one-dimensional (extended) Bose-Hubbard model; see Ref. [4].

A. Dynamical density-matrix renormalization group

In order to simulate the Bose-Hubbard type models using the (D)DMRG technique [15–17], the maximum number n_b of bosons per site should be limited, while each lattice site can be occupied, in principle, by infinitely many bosons. Nevertheless, the (D)DMRG results are unbiased and numerically exact as long as the dependence on n_b can be verified to be negligible. In the DDMRG scheme it makes a considerable difference from the correction vector method [14] to minimize the functional [16]

$$W_{A,\eta}(\omega,\psi) = \langle\psi|(E_0 + \omega - \hat{H})^2 + \eta^2|\psi\rangle + \eta\langle A|\psi\rangle + \eta\langle\psi|A\rangle, \tag{7}$$

where $|A\rangle = \hat{A}|\psi_0\rangle$. Then the imaginary part of the Green function can be evaluated as

$$W_{A,\eta}(\omega,\psi_{\min}) = -\pi\eta\,\mathrm{Im}\,G_A^{\mathrm{ret}}(\omega + i\eta). \tag{8}$$

Within this DDMRG scheme we repeat the sweeps in the finite-system algorithm until the functional $W_{A,\eta}(\omega,\psi)$ takes its minimal values.

Calculating the dynamical current [$A = J$ in Eqs. (7) and (8)] and kinetic-energy [$A = T$] correlation functions in the first Mott lobe of the Bose-Hubbard model, we keep $m = 800$ states to determine the ground state during the first five DMRG sweeps, and then use $m = 400$ states for the evaluation of the dynamical properties. For a precise analysis of the dynamical properties we consider a finite system with broadening width η as small as possible. In doing so artificial peaks can appear if η is too small for fixed system size L. Thus, one needs to find an appropriate $\eta(L)$ empirically. In order to avoid artificial peaks, in this paper we fix $\eta = 0.8t$ for $L = 64$.

B. Spectral broadening and deconvolution

The DDMRG method works with complex frequencies, i.e., instead of the real frequency ω, the calculations are done with a finite shift η into the complex plane: $\omega \to \omega + i\eta$. The shift to the complex plane introduces a Lorentzian spectral broadening of the correlation function, i.e., the DDMRG actually provides

$$S_A^\eta(\omega) = \frac{1}{\pi}\int_{-\infty}^{\infty} \frac{\eta}{(\omega - \widetilde{\omega})^2 + \eta^2} S_A(\widetilde{\omega}) d\widetilde{\omega} \tag{9}$$

at equally spaced frequencies ω_i with high numerical accuracy. The size of the intervals $\Delta\omega = |\omega_{i+1} - \omega_i|$ is smaller than, but of the order of η. Then, without loss of accuracy, the integration over ω in Eq. (9) can be represented by a matrix multiplication,

$$S_A^\eta(\omega_i) = \sum_j \frac{1}{\pi}\frac{\eta}{(\omega_i - \omega_j)^2 + \eta^2} S_A(\omega_j),$$
$$\underline{S_A^\eta} = \underline{\underline{L^\eta}} \cdot \underline{S_A}. \tag{10}$$

The derivation of the vector $\underline{S_A}$ for the correlation function at the frequencies ω_i from the corresponding DDMRG vector $\underline{S_A^\eta}$ ("deconvolution") poses an ill-conditioned inverse problem.

There is a number of deconvolution techniques for Lorentz-broadened spectra. It was shown in Refs. [18–20] that the matrix inversion of Eq. (10) provides a simple and reliable way to deconvolve spectral functions,

$$\underline{S_A} = (\underline{\underline{L^\eta}})^{-1} \cdot \underline{S_A^\eta}. \tag{11}$$

As seen from Eq. (2), the correlation functions are positive, $S_A(\omega) \geqslant 0$. However, the deconvolution scheme (11) cannot guarantee this so that the deconvolved correlation functions might be negative in some regions. The width and depth of the regions with negative values of the correlation functions can be taken as a sign of the error introduced by the deconvolution technique and the finite-size and finite-η limitations in the DDMRG method. Of course, the deviations are most prominent when the correlation functions tend to zero or show narrow extrema. In the first Mott lobe of the Bose-Hubbard model, the width of the peaks is large enough to deconvolve the data by using $\eta = 0.8t$ and $L = 64$. Then, only very close to $\omega \simeq \Delta$ (with particle gap Δ) do the spectra show negative values, as we see in the following.

C. Strong-coupling expansion

In the strong-coupling expansion we use a Harris-Lange transformation [21,22] to obtain an effective Hamilton operator $\hat{h}$ that does not mix states from different subspaces of the operator for potential energy $U\hat{D}$. Within this approach, the transformation operator $\hat{S}$ as well as the effective Hamilton operator $\hat{h}$ are expanded in x:

$$\hat{h} = e^{\hat{S}}\hat{H}e^{-\hat{S}} = U\hat{D} + t\sum_{r=0}^{\infty} x^r \hat{h}_r,$$
$$\hat{S} = -\hat{S}^\dagger = \sum_{r=1}^{\infty} x^r \hat{S}_r. \tag{12}$$

In mth order SC perturbation theory, the operators $\hat{h}_r$ and $\hat{S}_r$ are constructed iteratively whereby we enforce $[\hat{h}_r, \hat{D}]_- = 0$ for $0 \leqslant r \leqslant m$. This requires that we keep the operators up $\hat{S}_m$, $\hat{h}_{m-1}$ in the Taylor series for $\hat{S}$ and $\hat{h}$.

The (nondegenerate) ground state $|\Psi_0\rangle$ for finite x is obtained from the (nondegenerate) ground state $|\Phi_0\rangle$ for $x = 0$ as

$$|\Psi_0\rangle = \exp(-\hat{S})|\Phi_0\rangle. \tag{13}$$

Note that the ground state for $t = 0$ is very simple because for $N = L$ every site is singly occupied by a boson, $|\Phi_0\rangle = \prod_j \hat{b}_j^+|\text{vac}\rangle$. Within SC perturbation theory, the evaluation of a ground state expectation values of an operator $\hat{A}$ reduces to

$$\begin{aligned}\langle\Psi_0|\hat{A}|\Psi_0\rangle &= \langle\Phi_0|\tilde{A}|\Phi_0\rangle,\\ \tilde{A} &= \exp(\hat{S})\hat{A}\exp(-\hat{S}).\end{aligned} \tag{14}$$

To lowest order, it is readily deduced from Eq. (13) that the operator $\hat{S}_1$ generates states in $|\Phi_0\rangle$ with one doubly occupied site and a neighboring hole. In general, the states from the subspace $\mathcal{H}_1 \subset \mathcal{H}$ give rise to the primary Hubbard band in the dynamical correlation functions around $\omega \approx U$. In higher orders in Eq. (13), states from $\mathcal{H}_2$ and $\mathcal{H}_3$ appear in $|\Psi_0\rangle$ that give rise to the secondary and tertiary Hubbard bands. Therefore, as long as x is small and the spectral splitting of the Hilbert space is large, the dynamical correlation functions display contributions from energetically separated Hubbard bands. Due to sum rules and the fact that the correlation functions are non-negative, most of the spectral weight is concentrated in the primary Hubbard band. Within SC perturbation theory, the contributions from the higher Hubbard bands is fairly small.

For the primary Hubbard band in the mth-order approximation, we have to consider one double occupancy and one hole on a ring. When their relative distance is larger than m lattice sites, they do not interact with each other. For this reason, the SC problem reduces to the analytical solution of a two-particle problem with a finite-range interaction [11]. Most importantly, the interaction leads to a backscattering of the hole from the double occupancy so that an effective single-particle problem results where the hole moves on a chain with open boundary conditions.

For higher-order corrections the analytical expressions for the weights and the Hamilton operator are employed for the succeeding numerical evaluation of the correlation functions. If the states describe a single quasiparticle, Cauchy's integral formula can be used to compute the results for an infinite system [11,13] without spectral broadening, $\eta = 0^+$. The contributions originating from states with two or more quasiparticles can be obtained by a simple diagonalization of the Hamilton operator for systems large enough to set $\eta \approx 0$. However, since this perturbation theory is based on the spectral separation of the Hilbert space, it breaks down when the gap becomes exponentially small close to the Kosterlitz-Thouless-type Mott transition at $x_c \approx 0.305$. Therefore, its applicability is limited to $x \lesssim 0.10$, as we shall see below.

D. Results from field theory

Close to the Mott transition, the Bose-Hubbard model can be described by the sine-Gordon model where the dispersion of holons (h) and antiholons ($\bar{\text{h}}$) with momentum P is given by $E(P) = \pm[P^2 + (\Delta/2)^2]^{1/2}$ where Δ is the (exponentially small) single-particle gap. If only one holon and antiholon is taken into account and a marginal interaction between them is assumed, the two-particle contribution to the current-current correlation function is given by [23–25] ($\nu = \omega/\Delta$)

$$\begin{aligned}S_{J,\text{h},\bar{\text{h}}}(\omega) = \frac{\Delta}{\pi}C_2(\Delta)\frac{2}{\pi}\frac{\sqrt{\nu^2-1}}{\nu}\Theta(\nu-1)\\ \times\exp\left(-\int_0^\infty\frac{dx}{x}\frac{1-\cos(x\theta/\pi)\cosh x}{\exp(x/2)\cosh(x/2)\sinh x}\right),\end{aligned} \tag{15}$$

where $\theta = 2\text{arccosh}(\nu)$. Formula (15) is exact in the interval $\Delta \leqslant \omega \leqslant 2\Delta$. For $\omega > 2\Delta$ there are corrections to (15), which are due to multiholon and antiholon states and have a more complicated structure but can be shown to be important only at energies $\omega \gg \Delta$ [25], where the field-theory approach becomes invalid anyway.

The more general case with a relevant holon-antiholon interaction, parametrized by $1/2 < \beta^2 = K/2 < 1$, is discussed in detail in Ref. [8]; here, the parameter K in a Luttinger-model description or the parameter β^2 in the sine-Gordon model characterize the strength of the holon-antiholon interaction. As we shall see below, our DDMRG is not sufficient to determine the value β^2 for the first Mott lobe accurately but we shall see that the assumption $\beta^2 = 1$ as used in Eq. (15) provides a reasonable description of the DDMRG data for the frequency dependence of the current-current correlation function close to the gap (see below).

The current correlation function is finite only beyond the single-particle gap with a square-root onset at $\omega = \Delta$. It shows a maximum at $\omega \approx 1.24\Delta$ and a power-law decay at large frequencies. The normalization $C_2(\Delta)$ cannot be calculated analytically. To estimate the normalization $C_2(\Delta)$, we use the sum rule for the conductivity,

$$\int_0^\infty\frac{d\omega}{\pi}\text{Re}[\sigma(\omega)] = -\frac{1}{2L}\langle\Psi_0|\hat{T}|\Psi_0\rangle. \tag{16}$$

This quantity can be determined accurately by using the ground-state DMRG. For example, for $x = 0.20$ we find $[\Delta = 0.436t,\ -\langle\Psi_0|\hat{T}|\Psi_0\rangle/(2L) = 1.418t]$ and for $x = 0.15$ we find $[\Delta = 1.63t, -\langle\Psi_0|\hat{T}|\Psi_0\rangle/(2L) = 1.133t]$.

Close to the Mott transition, most of the optical weight is concentrated at low energy $\omega \sim \Delta$. Therefore, in the field-theory limit, the left-hand side of Eq. (16) can be determined from Eq. (15) because the omitted terms have a negligible contribution at low energy. This comparison provides $C_2(\Delta)$ for given x,

$$C_2(\Delta) = -\frac{\langle\Psi_0|\hat{T}|\Psi_0\rangle}{2L}\frac{\pi}{F\Delta}, \tag{17}$$

with

$$\begin{aligned}F &= \frac{2}{\pi}\int_1^\infty dy\frac{\sqrt{y^2-1}}{y^2}\\ &\quad\times\exp\left(-\int_0^\infty\frac{dx}{x}\frac{1-\cos(2x\text{arccosh}(y)/\pi)\cosh x}{\exp(x/2)\cosh(x/2)\sinh x}\right)\\ &\approx 1.70,\end{aligned} \tag{18}$$

with accuracy ± 0.01. Therefore, for $x = 0.20$, we have $C_2 = 6.01$ and, for $x = 0.15$, we find $C_2 = 1.28$.

The result from field theory is applicable in the region where the gap is (exponentially) small. Therefore, it is complementary to the DDMRG with its energy resolution $\eta \approx 12W/L$ where $W = 4t$ is the bare bandwidth. We note that the formula (15) works surprisingly well for the fermionic Hubbard model even when the gap is not exponentially small but of the order of t [26,27]. Therefore, we compare our DDMRG results for the current correlation function for $x = 0.20$ and $x = 0.15$ to those from field theory in Sec. III B.

III. CORRELATION FUNCTIONS

A. Strong-coupling result to leading order

To leading order in the SC expansion, the doubly occupied site and the hole only experience their hard-core repulsion. Otherwise, they move freely with hoping amplitudes $t_h = t$ for the hole and $t_d = -2t$ for the double occupancy. Consequently, both the current correlation function and the kinetic-energy correlation function are given by a semi-ellipse,

$$S^{(0)}_{J,T}(\omega) = \frac{4}{3\pi}\sqrt{1-\left(\frac{\omega-U}{6t}\right)^2}\,\Theta\left(1-\left(\frac{\omega-U}{6t}\right)^2\right), \quad (19)$$

where $\Theta(x)$ denotes the Heaviside step function (see also Refs. [6,7,11]). The result is qualitatively the same for the fermionic Hubbard model [26,27], where $t^{\mathrm{F}}_d = -t$.

The correlation function is finite only above the single-particle gap, $\Delta \approx U - 6t$ for $x \to 0$. Moreover, the correlation function displays a square-root onset, as seen in field theory. Therefore, the square-root onset above the single-particle gap apparently is a generic feature of the correlation functions in the Mott-insulating phase.

B. Current correlation function

In Fig. 1 we show the deconvolved DDMRG data and the results from sixth-order SC theory for the current correlation function for $x = 0.05$, 0.08, 0.10, and 0.12. For $x = 0.05$, the correlation function is almost an undisturbed semi-ellipse; see Eq. (19). Upon decreasing the interaction, the width of the primary Hubbard band increases, and spectral weight is shifted towards the lower band edge so that the current correlation function becomes asymmetric. As seen from the figure, both DDMRG and SC agree perfectly with each other up to $x = t/U = 0.08$. As discussed in Sec. II B, the slightly negative DDMRG data for the current correlation function close to the band edges are an artifact of the deconvolution scheme.

For smaller interactions, $x \geqslant 0.10$, the current correlation function steeply rises to its maximum value as a function of frequency and falls off monotonically beyond the maximum. The agreement of DDMRG and SC is satisfactory only at first glance because some wiggles appear in the SC results that are absent in the DDMRG data. The wiggles are more pronounced for $x = 0.12$ than for $x = 0.10$. The reason why these unphysical wiggles appear in SC is discussed in Appendix B.

For $x = 0.12$, the tertiary Hubbard band can be seen in the DDMRG data. In the SC theory this band emerges from states

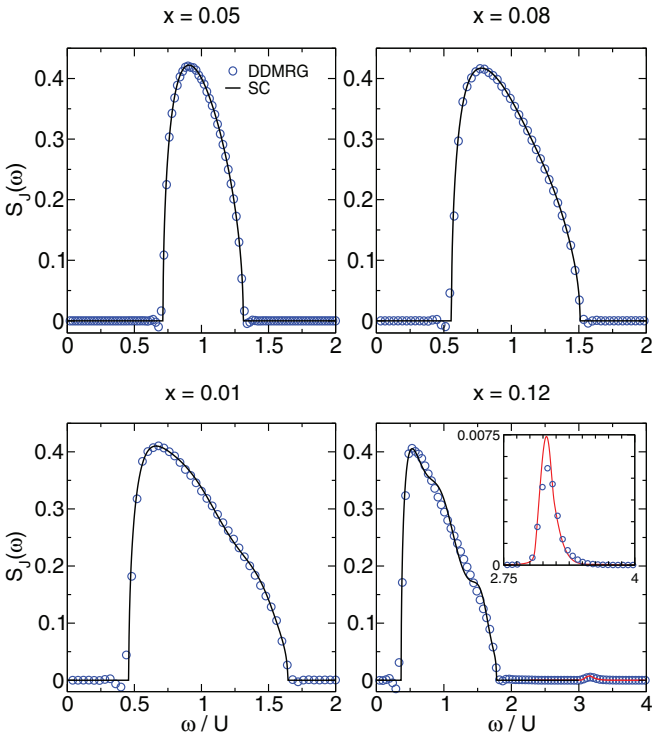

FIG. 1. (Color online) Current correlation function for interactions $x = t/U = 0.05, 0.08, 0.1, 0.12$ from top left to bottom right. The deconvolved DDMRG data (circles) were obtained for $L = 64$, PBCs, and $\eta = 0.8t$. The black solid lines give the result of the SC theory of the primary Hubbard band. The red solid lines give the result of the SC theory for the tertiary Hubbard band. A magnification of the tertiary Hubbard band is shown in the inset.

with a triple occupancy and two holes whose contributions to $|\tilde{J}|\Phi_0\rangle|^2$ are of the order $O(x^4)$. For $x = 0.12$ the weight of the primary, secondary, and tertiary Hubbard bands is given by 3.04, 1.5×10^{-3}, and 0.01, respectively. Here, the weight of the primary Hubbard band has been approximated by a sixth-order expansion, while a third- and fourth-order expansion has been used for the secondary and tertiary Hubbard band, respectively. The secondary Hubbard band is described by two double occupancies and two holes but is not visible because its weight is only of the order $O(x^6)$; see Appendix A.

To leading order, the total weight of the correlation functions is given by $\int_0^\infty S^{(0)}_{T,J}(\omega)d\omega = 4$. For $x > 0$, the total spectral weight can be determined by the static DMRG method with great precision so that it can be used as a test for the accuracy of the SC expansion. The results for the total weight from DMRG and SC deviate by less than 3×10^{-3} up to $x \leqslant 0.12$. For higher values of x, the SC theory seems to overestimate the weight.

For interaction parameters $x = 0.15$ and $x = 0.20$, only the DDMRG can provide reliable results. In Fig. 2 we plot the Lorentz-broadened current correlation function $S^{\eta}_J(\omega)$ for $\eta = 0.8t$ and compare it to the predictions from field theory. Even up to half the width of the primary Hubbard band, the field-theory curve agrees with the DDMRG data, despite the fact that the gap is quite sizable for $x = 0.15$. For $x = 0.20$, the agreement appears to be worse than for $x = 0.15$. At $x = 0.20$,

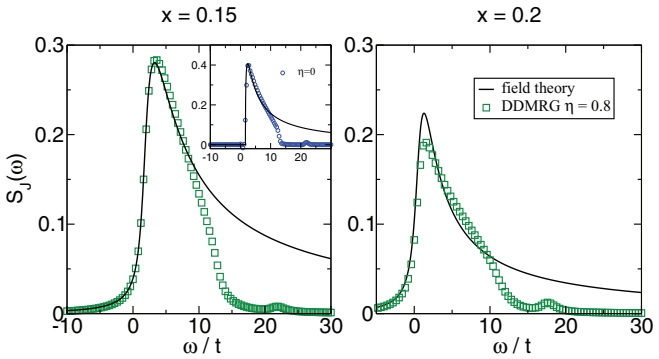

FIG. 2. (Color online) DDRMG data (squares) for $L = 64$, PBCs, and $\eta = 0.8t$ for (left panel) $x = 0.15$ and (right panel) $x = 0.2$. The solid black line gives the Lorentz-broadened field-theoretical results. The deconvolved DDMRG data (circles) and the field-theory results are shown in the inset for $x = 0.15$.

however, the DDMRG has difficulties to resolve the quite sharp maximum close to the onset of the correlation function. Here, larger system sizes and, correspondingly, smaller values for η would improve the agreement. Therefore, we show exemplarily a comparison of the deconvolved DDMRG data with the field-theory results in the inset of Fig. 2 for $x = 0.15$ and omit a further deconvolution of the DDMRG data in this parameter regime.

C. Kinetic correlation function

Before we discuss $S_T(\omega > 0)$, we briefly comment on the weight at $\omega = 0$. Within the SC expansion to sixth order, it is given by

$$\sqrt{w_0^T} = 8x - 16x^3 + \frac{529}{3}x^5 + O(x^7). \tag{20}$$

Apparently, the series converges rapidly even for $x = 0.2$. In general, the SC expansion reproduces the total weight of the kinetic-energy correlation function with an accuracy of 3.7×10^{-2} for $x \leqslant 0.12$. As for the current correlation function, the SC expansion seems to overestimate the weight for higher values of x.

In Fig. 3 we show the kinetic-energy correlation function for the values $x = 0.05$, 0.08, 0.1, and 0.12. For $x \leqslant 0.08$ the agreement of SC and DDMRG is very good. For $x = 0.1$ and 0.12, the sixth-order SC theory starts to develop wiggles as in the case of the current correlation functions, which are not seen in the DDMRG data. Therefore, the SC expansion cannot be used beyond $x = 0.10$. As the current correlation function, the kinetic-energy correlation function is finite above the single-particle gap with a square-root onset. In contrast to the current correlation function, the primary Hubbard band for S_T appears to remain symmetrical so that its maximum appears in the middle of the band for all interaction strengths.

The total weight of the secondary and tertiary Hubbard bands are of the order $O(x^6)$ and $O(x^2)$. For $x = 0.12$, the weight of the primary, secondary, and tertiary Hubbard bands is given by 3.3, 3.3×10^{-3}, and 0.076, respectively. The operator $\hat{T}$ is symmetric under spatial inversion, so that states in which the holes are symmetrically placed to the left and the

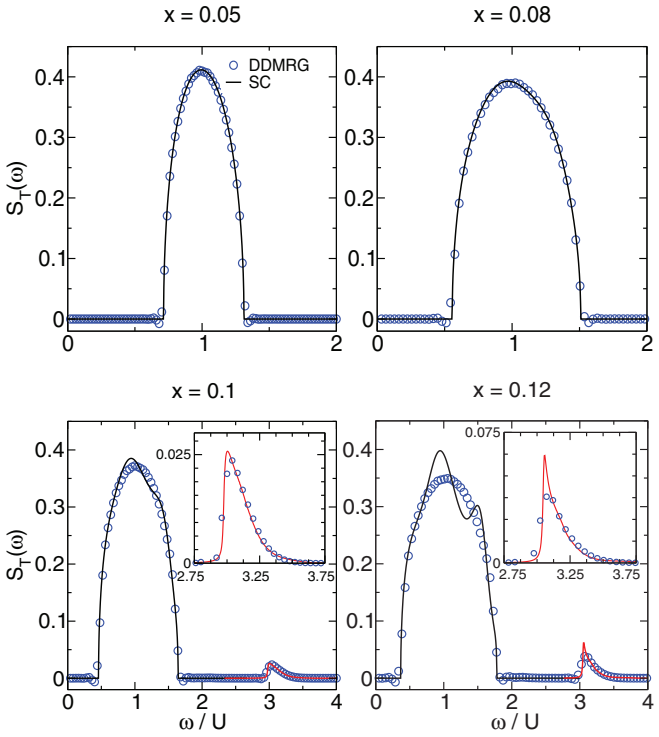

FIG. 3. (Color online) Kinetic-energy correlation function for interactions $x = 0.05,0.08,0.1,0.12$ (from top left to bottom right). The deconvolved DDMRG data (circles) were obtained for $L = 64$, PBCs, and $\eta = 0.8t$. Black solid lines gives the result of the SC theory of the primary Hubbard band. Red solid line gives the result of the SC theory for the tertiary Hubbard band. A magnification of the tertiary Hubbard band is shown in the insets.

right of the triple occupancy also occur in $\tilde{T}|\Phi_0\rangle$. They are the leading-order contributions to the tertiary Hubbard band. Therefore, the tertiary Hubbard band is more prominent in S_T than in S_J where the spatial antisymmetry eliminates these states; see Appendix A.

In Fig. 3, we also compare the DDMRG data with SC results for the tertiary Hubbard band. Note, however, that the calculations are quite cumbersome so that we used the weights of the tertiary Hubbard band up to fourth order and considered the action of the effective Hamiltonian on $\mathcal{H}_3$ in second order only. This means that we work with $\hat{S}_4$ and $\hat{h}_1$. Given these simplifications, we obtain the SC results for the tertiary Hubbard band from an exact diagonalization of a system of $L = 128$ lattice sites and a very small spectral broadening of $\eta = 0.08$. Despite these limitations, our restricted SC approach quite accurately describes the asymmetrical shape of the tertiary Hubbard band.

The third Hubbard band shows some interesting features. For example, an attractive force acts between the two particles if they are placed next to each other. Moreover, the alignment of a hole next to the triple occupancy leads to a decrease in the potential energy. These effects induce sizable correlations between the holes and the triple occupancy which influences the shape of the correlation function.

For interaction parameters $x = 0.15$ and $x = 0.20$, only the DDMRG can provide reliable results. In Fig. 4 we plot

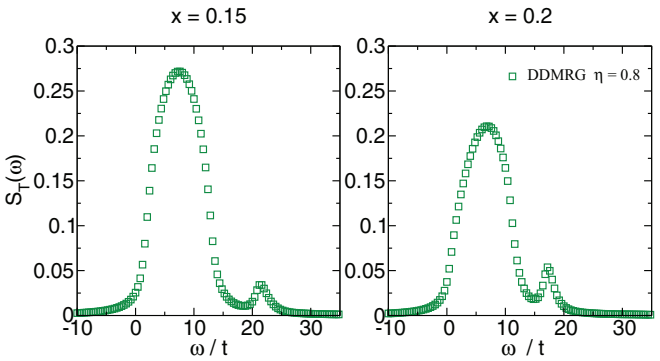

FIG. 4. (Color online) DDRMG data (squares) were obtained for $L = 64$, PBCs, and $\eta = 0.8t$ for (left panel) $x = 0.15$ and (right panel) $x = 0.2$.

the Lorentz-broadened kinetic-energy correlation function for $\eta = 0.8t$. The weight of the primary Hubbard band shrinks when we approach the transition whereas the tertiary Hubbard band gains more weight as a function of x. Therefore, the tertiary Hubbard band becomes clearly visible for $x = 0.20$.

IV. CONCLUSION AND OUTLOOK

In this work we calculated the current and kinetic-energy correlation functions for the Mott insulating regime of the one-dimensional Bose-Hubbard model at filling $\rho = N/L = 1$ using the strong-coupling (SC) expansion up to sixth order in $x = t/U$ and the dynamical density-matrix renormalization group (DDMRG) method on rings with $L = 64$ lattice sites. The DDMRG data for finite $\eta = 0.8t$ permit a reliable deconvolution of the Lorentz-broadened data so that the correlation functions can be studied in the thermodynamical limit.

A comparison of sixth-order SC and DDMRG results shows that SC is reliable up to $x = 0.10$. DDMRG on $L = 64$ sites can be used up to $x \lesssim 0.20$. For $x \gtrsim 0.20$ it becomes difficult to resolve the sharp maximum in the current correlation functions at frequency $\omega \approx 1.3\Delta$, where Δ is the single-particle gap. In any case, the exponentially small gap close to the Mott transition at $x_c \approx 0.305$ cannot be resolved by (D)DMRG for $x \gtrsim 0.25$.

The correlation functions are dominated by the primary Hubbard band around $\omega \approx U$. The primary Hubbard band starts at the single-particle gap with a characteristic square-root onset $S_{J,T}(\omega \to \Delta) \propto \sqrt{\omega - \Delta}$. This is seen in SC perturbation theory and in the deconvolved DDMRG data. It is confirmed for the current correlation function by field theory which is applicable close to the Mott transition. Apart from a maximum at low frequencies, the primary Hubbard band of the current correlation function is featureless. The primary Hubbard band of the kinetic-energy correlation function appears to be symmetric with a single maximum at the band center. For both correlation functions, the secondary Hubbard band is very small but the tertiary Hubbard band around $\omega = 3U$ becomes visible for $x \gtrsim 0.10$. The asymmetric shape is understood from SC theory which includes correlations between the quasiparticles.

For the primary Hubbard band in the one-dimensional Bose-Hubbard model, the attractive correlations between doubly occupied site and hole are not significant enough to overcome their hard-core repulsion. Therefore, it requires a finite nearest-neighbor interaction to generate an excitonic state [4,26,27]. The situation could change in the two-dimensional Bose-Hubbard model. In recent quantum Monte Carlo studies and field-theoretical studies [28], the existence of a peak in the optical conductivity has been alluded to in the critical region above but close to the Mott transition, $x_c^{2d} - x < 1.15x_c^{2d}$. This peak is a signature of the Higgs boson in the two-dimensional superfluid which should persist as a resonance in the Mott phase.

Albeit the SC expansion is better behaved in two than in one dimension [29], it is not clear at this point whether the expansion can be carried out far enough to include such features. The SC diagrams show that higher orders in the expansion generate an attractive interaction between the quasiparticles in the primary and tertiary Hubbard band. However, it is unclear whether these interactions are sufficient to generate a resonance structure close to the transition. Moreover, the diagrammatic expansion is considerably more cumbersome in two dimensions than in one dimension. Therefore, a SC study of the two-dimensional Bose-Hubbard model remains an open problem.

ACKNOWLEDGMENTS

S.E. and H.F. gratefully acknowledge financial support by the Deutsche Forschungsgemeinschaft through SFB 652.

APPENDIX A: DIAGRAMMATIC ANALYSIS

The Taylor expansion for $\hat{h}$ in Eq. (12) gives rise to so-called *process chains* [29–31]. They represent sequences that involve alternately the kinetic-energy operator $\hat{T}$ and projection operators $\hat{P}_D$ onto subspaces $\mathcal{H}_D$. For example, the leading-order approximations of the transformation operator $\hat{S}$ and the effective Hamilton operator $\hat{h}$ can be written as

$$U\hat{D} + t\hat{h}_0 = U\hat{D} + t\sum_D \hat{P}_D\hat{T}\hat{P}_D, \tag{A1}$$

$$\hat{S}_1 = \sum_{D_1,D_2} \frac{\hat{P}_{D_1}\hat{T}\hat{P}_{D_2}}{D_1 - D_2}. \tag{A2}$$

This example shows that each process chain must be weighted according to the number of double occupancies that occur in intermediate steps.

The application of the Baker-Campbell-Hausdorff formula to Eqs. (12) shows that $\hat{h}$ and $\hat{S}$ can be written in terms of nested Lie brackets. In this way, only connected hopping processes must be considered in the action of these operators onto some state. This simplification leads to an intuitive understanding of why the secondary Hubbard band has vanishingly small intensity. Its starting state consists of two double occupancies and two holes. The leading-order contribution for the secondary Hubbard band can be depicted as

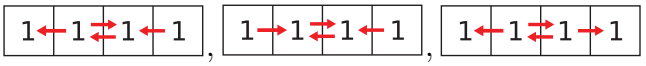

The actual computation of these diagrams requires the evaluation of all possible hopping processes generated by an

arbitrary time ordering of its constituents. One hopping process originates from the operator $\hat{T}$ or $\hat{J}$ itself while the other processes result from $\hat{S}_3$ so that these states are $O(x^3)$. Note that the antisymmetry of $\hat{J}$ with respect to spatial inversion leads to a cancellation of the last two diagrams.

APPENDIX B: LIMITATIONS OF STRONG-COUPLING EXPANSION

In the primary Hubbard band, a particle hole-pair is created in which the hole is placed n lattice sites to the right or left of the double occupancy (state $|\pm n\rangle$). In the lowest-order approximation, the hole cannot jump over the double occupancy, so that it moves on an open chain on the remaining $L-1$ sites. The correlation functions are a weighted sum of Green functions of the form $G_{ij}(\omega) = \langle i|\delta(\omega - (\hat{h} - E_0))|j\rangle$.

For $x \geqslant 0.1$, the SC expansion shows some wiggles which can be understood as follows: In general, the Greens functions G_{jj} or G_{1j} of a particle in an open chain subject to nearest-neighbor hopping with lattice-site index j will have j extrema. The parts of the state $\tilde{J}|\Phi_0\rangle$ that describe particle-hole pairs which are separated by j lattice sites thus lead to contributions in $S_J(\omega)$ which have j maxima. The wiggles naturally appear when the expansion parameter x is chosen too large so that the weight of these contributions is overestimated and not yet corrected by contributions to higher orders.

[1] I. Bloch, J. Dalibard, and W. Zwerger, Rev. Mod. Phys. **80**, 885 (2008).
[2] J. Dalibard, F. Gerbier, G. Juzeliūnas, and P. Öhberg, Rev. Mod. Phys. **83**, 1523 (2011).
[3] J. Struck, C. Ölschläger, M. Weinberg, P. Hauke, J. Simonet, A. Eckardt, M. Lewenstein, K. Sengstock, and P. Windpassinger, Phys. Rev. Lett. **108**, 225304 (2012).
[4] T. D. Kühner, S. R. White, and H. Monien, Phys. Rev. B **61**, 12474 (2000).
[5] J.-W. Huo, F.-C. Zhang, W. Chen, M. Troyer, and U. Schollwöck, Phys. Rev. A **84**, 043608 (2011).
[6] S. Ejima, H. Fehske, and F. Gebhard, Europhys. Lett. **93**, 30002 (2011).
[7] A. Tokuno and T. Giamarchi, Phys. Rev. Lett. **106**, 205301 (2011); The analytic expression for the leading order of the correlation functions can already be extracted from the results presented in this work. However, our band width seems to be twice as large, which might be caused by a wrong scaling of t. Note also the different values for x_c.
[8] A. Iucci, M. A. Cazalilla, A. F. Ho, and T. Giamarchi, Phys. Rev. A **73**, 041608 (2006).
[9] C. Kollath, A. Iucci, I. P. McCulloch, and T. Giamarchi, Phys. Rev. A **74**, 041604 (2006).
[10] G. D. Mahan, *Many-Particle Physics* (Kluwer, New York, 2000).
[11] S. Ejima, H. Fehske, F. Gebhard, K. zu Münster, M. Knap, E. Arrigoni, and W. von der Linden, Phys. Rev. A **85**, 053644 (2012).
[12] S. Ejima, H. Fehske, and F. Gebhard, J. Phys.: Conf. Ser. **391**, 012031 (2012).
[13] S. Ejima, F. Lange, H. Fehske, F. Gebhard, and K. zu Münster, Phys. Rev. A **88**, 063625 (2013).
[14] T. D. Kühner and S. R. White, Phys. Rev. B **60**, 335 (1999).
[15] S. R. White, Phys. Rev. Lett. **69**, 2863 (1992).
[16] E. Jeckelmann, Phys. Rev. B **66**, 045114 (2002).
[17] E. Jeckelmann and H. Fehske, Riv. Nuovo Cimento Soc. Ital. Fis. **30**, 259 (2007).
[18] F. Gebhard, E. Jeckelmann, S. Mahlert, S. Nishimoto, and R. M. Noack, Eur. Phys. J. B **36**, 491 (2003).
[19] S. Nishimoto and E. Jeckelmann, J. Phys.: Condens. Matter **16**, 613 (2004).
[20] M. Paech and E. Jeckelmann, Phys. Rev. B **89**, 195101 (2014).
[21] A. B. Harris and R. V. Lange, Phys. Rev. **157**, 295 (1967).
[22] P. G. J. van Dongen, Phys. Rev. B **49**, 7904 (1994).
[23] M. Karowski and P. Weisz, Nucl. Phys. B **139**, 455 (1978).
[24] F. A. Smirnov, *Form Factors in Completely Integrable Models of Quantum Field Theory* (World Scientific, Singapore, 1992).
[25] D. Controzzi, F. H. L. Essler, and A. M. Tsvelik, Phys. Rev. Lett. **86**, 680 (2001).
[26] E. Jeckelmann, F. Gebhard, and F. H. L. Essler, Phys. Rev. Lett. **85**, 3910 (2000).
[27] F. H. L. Essler, F. Gebhard, and E. Jeckelmann, Phys. Rev. B **64**, 125119 (2001).
[28] L. Pollet and N. Prokofev, Phys. Rev. Lett. **109**, 010401 (2012).
[29] N. Teichmann, D. Hinrichs, M. Holthaus, and A. Eckardt, Phys. Rev. B **79**, 224515 (2009).
[30] A. Eckardt, Phys. Rev. B **79**, 195131 (2009).
[31] B. Damski and J. Zakrzewski, Phys. Rev. A **74**, 043609 (2006).